Vented hydrogen deflagrations in 20-foot ISO containers

Trygve Skjold

E-mail: *trygve@gexcon.com*

Gexcon, Fantoftvegen 38, 5072 Bergen, Norway

Abstract

This paper summarises results from 66 vented hydrogen deflagration experiments performed in 20-foot ISO containers: 42 tests with initially homogeneous and quiescent mixtures, and 24 tests with inhomogeneous mixtures. The work was part of the project *Improving Hydrogen Safety for Energy Applications through pre-normative research on vented deflagrations* (HySEA). The discussion highlights some of the implications of the results with respect to safe implementation of explosion venting protective systems and devices for hydrogen applications.

Keywords: *hydrogen safety, vented deflagrations, structural response, containers*

1. Introduction

1.1 The HySEA project

Fires and explosions represent a significant hazard for hydrogen installations (Skjold *et al.*, 2018a), and specific measures are generally required for reducing the risk to a tolerable level (Skjold *et al.*, 2017a). Explosion venting is a frequently used measure for reducing the consequences of deflagrations in confined systems. However, vented deflagrations are inherently complex phenomena, and it is not straightforward to develop accurate models for predicting the consequences of potential accidents. The main objective of the project *Improving Hydrogen Safety for Energy Applications through pre-normative research on vented deflagrations* (HySEA) was to develop recommendations for improved international standards for the design of explosion venting devices, such as EN 14994 (2007) and NFPA 68 (2018).

The members of the HySEA consortium were Gexcon (coordinator), University of Warwick (UWAR), University of Pisa (UNIPI), Fike Europe, Impetus Afea and Hefei University of Technology (HFUT). The research activities in the project were organised in five work packages (WPs), and included evaluation, development and validation of empirical or semi-empirical models (Sinha *et al.*, 2018; Lakshmipathy *et al.*, 2018), vented deflagration experiments in containers (Skjold *et al.*, 2017b; Skjold *et al.*, 2018b) and smaller enclosures (Schiavetti *et al.*, 2018; Carcassi *et al.*, 2018), as well as development and validation of computational fluid dynamics (CFD) tools (Hisken *et al.*, 2016; Rao *et al.*, 2018; Skjold *et al.*, 2018cd) and finite element (FE) models (Pini *et al.*, 2018; Atanga *et al.*, 2018).

This paper summarises the results from 66 vented hydrogen deflagration experiments conducted in 20-foot ISO containers (Skjold *et al.*, 2018b). The 34 tests in the first experimental campaign focused on homogeneous mixtures. The 32 tests in the second campaign included tests with stratified mixtures, but also tests with initial turbulence generated by a fan, transient releases from pressurised vessels and selected reference tests with homogeneous mixtures.

2 Experiments

Gexcon performed the experiments at the remote test site on the island of Sotra outside Bergen in two experimental campaigns: tests 1-34 and tests 35-72. Twelve containers from the same manufacturing series were damaged beyond repair in 66 vented deflagration tests. The scenarios investigated included 42 tests with initially homogeneous and quiescent mixtures (14 tests vented through the doors, one test with closed container, and 27 tests vented through openings on the roof), and 24 tests with inhomogeneous mixtures (17 tests with stratified mixtures and seven tests with initial turbulence generated by either a fan or a transient jet). The total number of tests was 72, which included five unignited tests (tests 39-46) and one failed test (test 58).

Skjold *et al.* (2017b; 2018b) summarise previous work on vented deflagrations and describe the experimental setup and selected results. Table 1 summarises the experimental matrix for the 66 vented deflagration tests. The table includes information on the following variables:

- Test number and container number (C#) – test numbers in bold indicate the last test for a container, i.e. tests where the containers were severely damaged.
- Hydrogen concentration (C_{H2}), where an asterisk (*) indicates nominal concertation values for tests that involved inhomogeneous mixtures.
- Vent area (A_v), not including unintended openings caused by structural deformation.
- Type of venting device: 0.2 mm polyethylene in door opening (D), 0.2 mm perforated polyethylene covering 1-m^2 vent openings in the roof (O), commercial single-sheet bulged vent panels covering 1-m^2 vent openings in the roof (P), venting through initially closed container doors (C), and closed container subjected to quasi-static pressure load (S).
- Ignition position: back wall centre (bc), back wall upper (bu), and floor centre (fc).
- Obstacle configuration: frame only (FO), bottle basket in inner position (B1), pipe rack in inner position (P1), pipe rack in centre position (P2), pipe rack in inner position and bottle basket in outer position (P1B3), and high congestion (HC, i.e. P1B3 + additional obstacles).
- Flow conditions: initially quiescent (Q), local turbulence generated by fan (TF), transient jet from high-pressure reservoir (TJ), stratified mixture generated by 18 mm diameter jet release (SJ), and stratified mixture generated by 0.2 m x 0.2 m diffusive release (SD).
- Additional comments: tests part of first or second blind-prediction benchmark study (BP-1 and PB-2, respectively), only four or five out of six vent panels opened (4/6 and 5/6), etc.

Skjold *et al.* (2018b) and Skjold (2018) describe the experiments in more detail.

3 Data processing

The measured time series were smoothed with a digital filter (Savitzky & Golay, 1964), and the effect of varying the filter frequency was investigated (Skjold *et al.*, 2018b). Oscillations associated with alternating current at the frequency of the mains electricity (50 Hz) were processed with a digital filter in MATLAB™, and the filtered data were used when visual inspection of the plotted data and a frequency spectrum generated by fast Fourier transform (FFT) showed that the filtering had the desired effect. The problems associated with noise and drift were most severe for the weakest explosions, and several pressure measurements were discarded during the data analysis process. Due to the symmetry in the placement of the internal pressure sensors (Skjold *et al.*, 2018b), it was possible to identify and exclude obviously corrupt signals. There is nevertheless some inherent uncertainty associated with noise and drift in the signals. Figure 1 to Figure 9 documents the data processing in detail for test no. 60 (example). The final report from the experimental campaigns in 20-foot ISO containers includes the corresponding plots from all the 66 vented explosion tests (Skjold, 2018).

Table 1: Experimental matrix sorted by test number (continues on next page).

Test	C#	C_{H2} (vol.%)	A_v (m^2)	Vent.	Ign.	Obst.	Flow	Comments
1	1	15	5.56	D	bc	FO	Q	First blind-prediction
2	1	15	5.56	D	bc	FO	Q	First blind-prediction
3	1	15	5.56	D	bc	B1	Q	First blind-prediction
4	1	15	5.56	D	bc	B1	Q	First blind-prediction
5	1	15	5.56	D	bc	FO	Q	First blind-prediction
6	1	15	5.56	D	bc	B1	Q	First blind-prediction
7	1	21	5.56	D	bc	B1	Q	
8	1	24	5.56	D	bc	B1	Q	
9	1	24	5.56	C	bc	B1	Q	Doors initially closed
10	2	18	5.56	D	bc	B1	Q	
11	2	15	5.56	D	bc	P1	Q	
12	2	18	5.56	D	bc	P1	Q	
13	2	21	5.56	D	bc	P1	Q	
14	2	21	5.56	D	bc	P1B3	Q	
15	3	21	8.0	P	fc	FO	Q	
16	3	21	8.0	O	fc	FO	Q	
17	3	21	8.0	O	fc	P2	Q	
18	3	21	8.0	P	fc	P2	Q	
19	3	24	8.0	O	fc	P2	Q	
20	3	24	8.0	P	fc	P2	Q	
21	4	21	6.0	O	fc	FO	Q	
22	4	21	6.0	O	fc	P2	Q	
23	4	24	6.0	O	fc	P2	Q	
24	4	21	4.0	O	fc	P2	Q	
25	4	21	4.0	O	fc	FO	Q	
26	4	21	6.0	P	fc	FO	Q	
27	4	21	6.0	P	fc	P2	Q	
28	4	24	6.0	P	fc	P2	Q	
29	5	24	4.0	O	fc	P2	Q	
30	5	21	8.0	P	fc	P2	Q	
31	5	21	6.0	P	fc	P2	Q	
32	5	21	4.0	P	fc	FO	Q	
33	5	21	4.0	P	fc	P2	Q	
34	5	42	8.0	O	fc	P2	Q	Plastic: 42 vol.% H_2
35	6	18	8.0	O	fc	P2	TF	First test of second campaign

Test	C#	C_{H2} (vol.%)	A_v (m^2)	Vent.	Ign.	Obst.	Flow	Comments
36	6	21	8.0	O	fc	P2	TF	
37	6	21	6.0	O	fc	P2	TF	
38	6	21	4.0	O	fc	P2	TF	
44	6	21*	6.0	P	bu	FO	SD	
45	7	21	6.0	O	bu	FO	Q	
46	7	21	6.0	P	bu	FO	Q	
47	7	21	6.0	P	bu	FO	Q	
48	7	21	6.0	P	bu	P2	Q	
49	7	18*	6.0	P	bu	P2	SD	
50	7	18*	6.0	P	bu	P2	SJ	
51	7	18*	6.0	O	bu	P2	SJ	
52	7	18*	6.0	O	bu	P2	SD	
53	7	18*	6.0	O	bu	FO	SD	
54	7	18*	6.0	O	bu	FO	SJ	
55	7	18*	6.0	P	bu	FO	SJ	
56	7	18*	6.0	P	bu	FO	SD	
57	7	21*	6.0	P	bu	FO	SJ	Second blind-prediction
59	8	21*	6.0	P	bu	FO	SJ	Second blind-prediction
60	8	21*	6.0	P	bu	P2	SJ	Second blind-prediction
61	9	21*	6.0	P	bu	P2	SJ	Second blind-prediction
62	10	15*	6.0	P	bu	P2	SJ	
63	10	15*	5.0	P	bu	P2	SD	Five out of six panels opened
64	10	15*	6.0	P	bu	FO	SD	
65	10	15*	6.0	P	bu	FO	SJ	
66	10	15*	4.0	P	bu	FO	TJ	Four out of six panels opened
67	10	18*	4.0	P	bu	FO	TJ	Four out of six panels opened
68	10	21*	6.0	P	bu	FO	TJ	
69	10	42	8.0	P	fc	P2	Q	Panels: 42 vol.% H_2
70	11	12	0.0	S	bu	FO	Q	Quasi-static loading
71	12	12	6.0	P	fc	HC	Q	High-congestion
72	12	15	6.0	P	fc	HC	Q	High-congestion

Figure 1 shows the filtered (red and black lines) and unfiltered (orange and grey lines) pressure-time histories measured by pressure sensors P01-P2 (a) and P03-P04 (b) for test no. 60 (example). The smoothing frequency (SF) was 50 Hz, as indicated in the plots. The yellow star, in this and subsequent plots, indicates the time of ignition ($t = 0$) at ambient pressure, the yellow squares indicate the pressures P_{stat} when the vent panels start to open (at time t_{stat}), the yellow circles indicate the maximum rate of pressure rise $(dP/dt)_m$ for the filtered data series, and the

yellow triangles indicates maximum reduced explosion pressure P_m for the filtered data series. The blue plus signs indicate the P_m values for the other internal pressure measurements (i.e. P03-P08 in Figure 1a and P01-P02 as well as P04-P08 in Figure 1b), and the blue asterisks indicates the maximum pressures measured by the three external blast gauges (P09-P11) after filtering. The vertical dash-dotted magenta, green and cyan lines indicate the time when the hinged panels started to open (t_{stat}), and when the panels were approximately 45° (t_{45}) and 90° (t_{90}) open, respectively. Only the magenta line is included for tests where polyethylene was used as the venting device. The opening times for the panels were estimated based on visual observations of high-speed video recordings. Furthermore, in some of the tests the panels did not open simultaneously. As such, the time estimates entail a certain element of uncertainty.

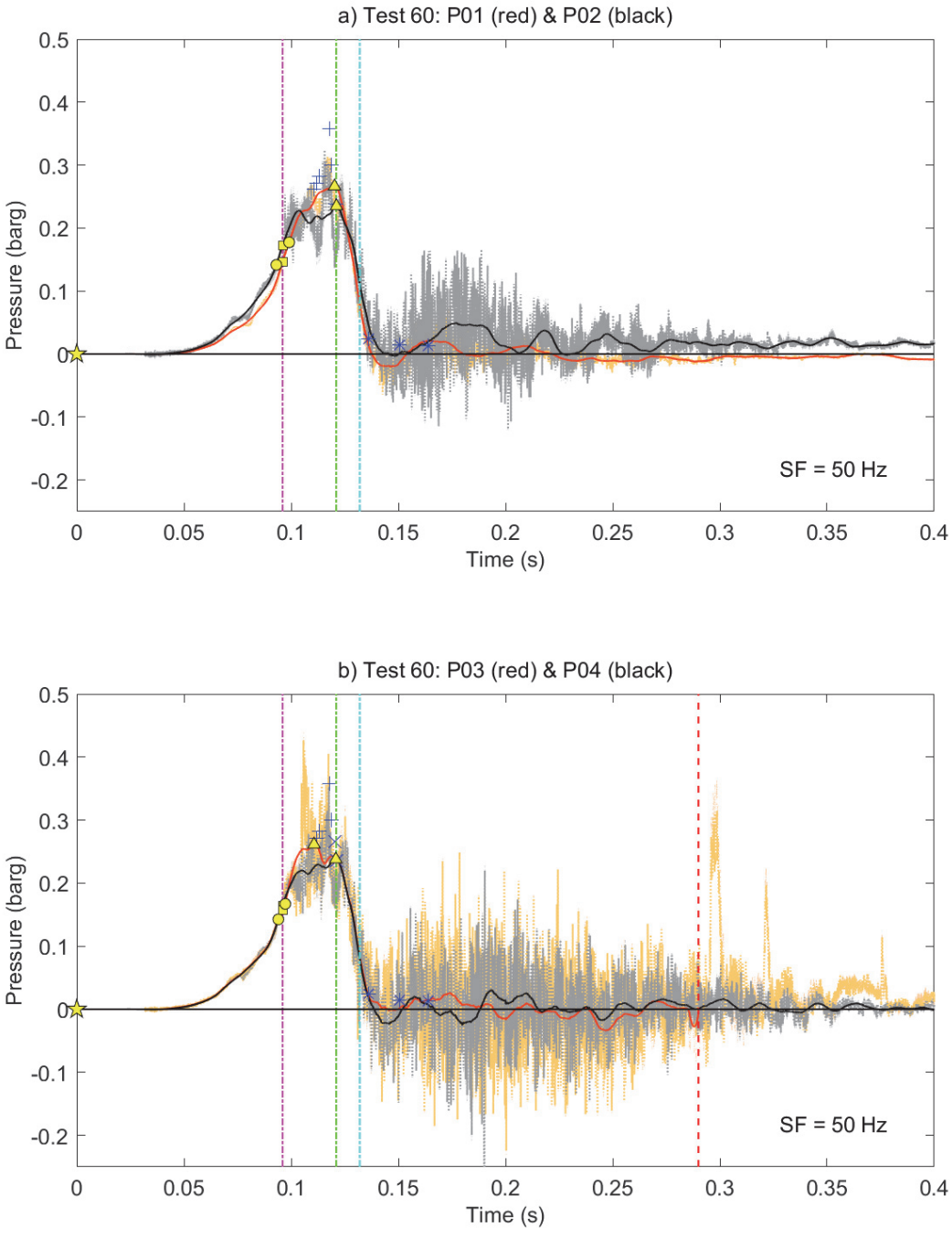

Figure 1: Filtered and unfiltered pressure-time histories (P01-P04) for test no. 60.

Figure 2 shows the pressure-time histories measured by pressure sensors P05-P06 (a) and P07-P08 (b) for test no. 60 (example), corresponding to the plots for sensors P01-P04 in Figure 1. The vertical dotted red line in Figure 1 b) and the vertical dotted black line in Figure 2 b) indicate the time when the remaining part of the signals from sensors P03 and P08, respectively, were discarded during the post-processing of data due to severe drift and/or noise. For some tests, one or several signals were discarded before the maximum rate of pressure rise and/or the maximum explosion pressure had occurred, and these parameters could therefore not be determined for all tests. Missing or undefined values are indicated by NaN ('not a number') or a long dash (—) in the tables that summarise results.

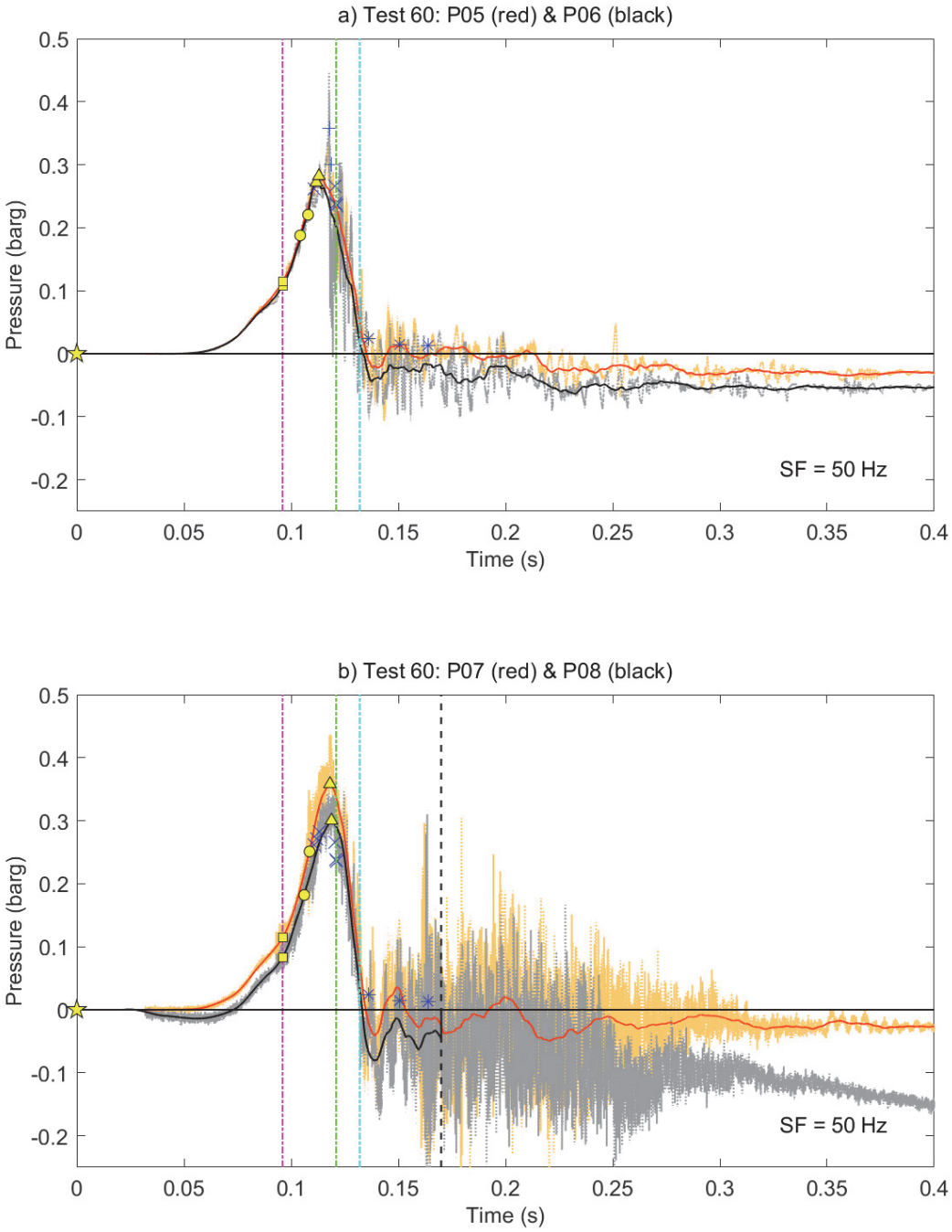

Figure 2: Filtered and unfiltered pressure-time histories (P05-P08) for test no. 60.

Figure 3 (a) shows the filtered (red, green and blue) and unfiltered (magenta, light green and light blue) pressure-time histories measured by the external blast gauges P09-P11 for test no. 60 (example). The triangles indicate maximum values for the smoothed data series. Figure 3 (b) shows the filtered (red and blue lines) and unfiltered (magenta and light blue lines) measurements of the displacement sensors D01 and D02. The red and light blue triangles indicate the maximum deflection D_m for D01 and D02, respectively. The vertical dash-dotted magenta, green and cyan lines indicate t_{stat}, t_{45} and t_{90}, respectively. The results from the displacement measurements were not particularly sensitive to the smoothing frequency (Skjold *et al.*, 2018b), and the smoothing frequency (SF) for the displacement measurements was set to twice the frequency of the pressure measurements.

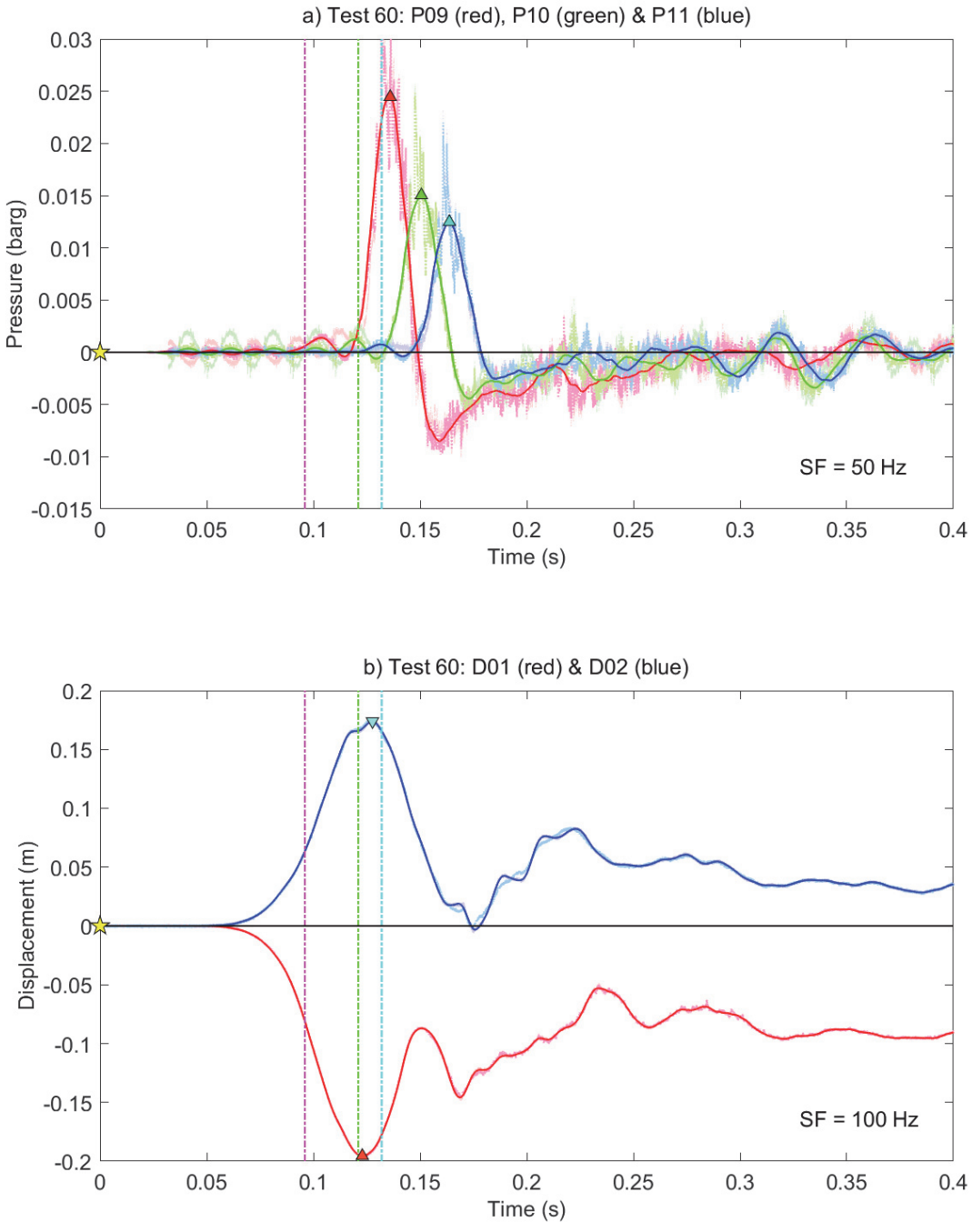

Figure 3: Filtered and unfiltered pressure-time and displacement-time histories for test no. 60.

Figure 4 shows the power spectra from the pressure-time histories measured by the internal pressure sensors P01-P08 (a) and the external blast gauges P09-P11 (b), as well as the displacement-time histories measured by the two displacement sensors D01-D02 (c) for test no. 60 (example). The logical values 'filter used' (FU) indicate whether the filtered data were used in further analysis. In most cases, including this example, the filtered data were only used for the measurements of external blast pressures (P09-P11), where the digital filter reduces the noise from the 50 Hz mains significantly. The reduced level of noise is clearly visible during the initial phase of the pressure-time histories for P09 and P10 shown in Figure 3 (a).

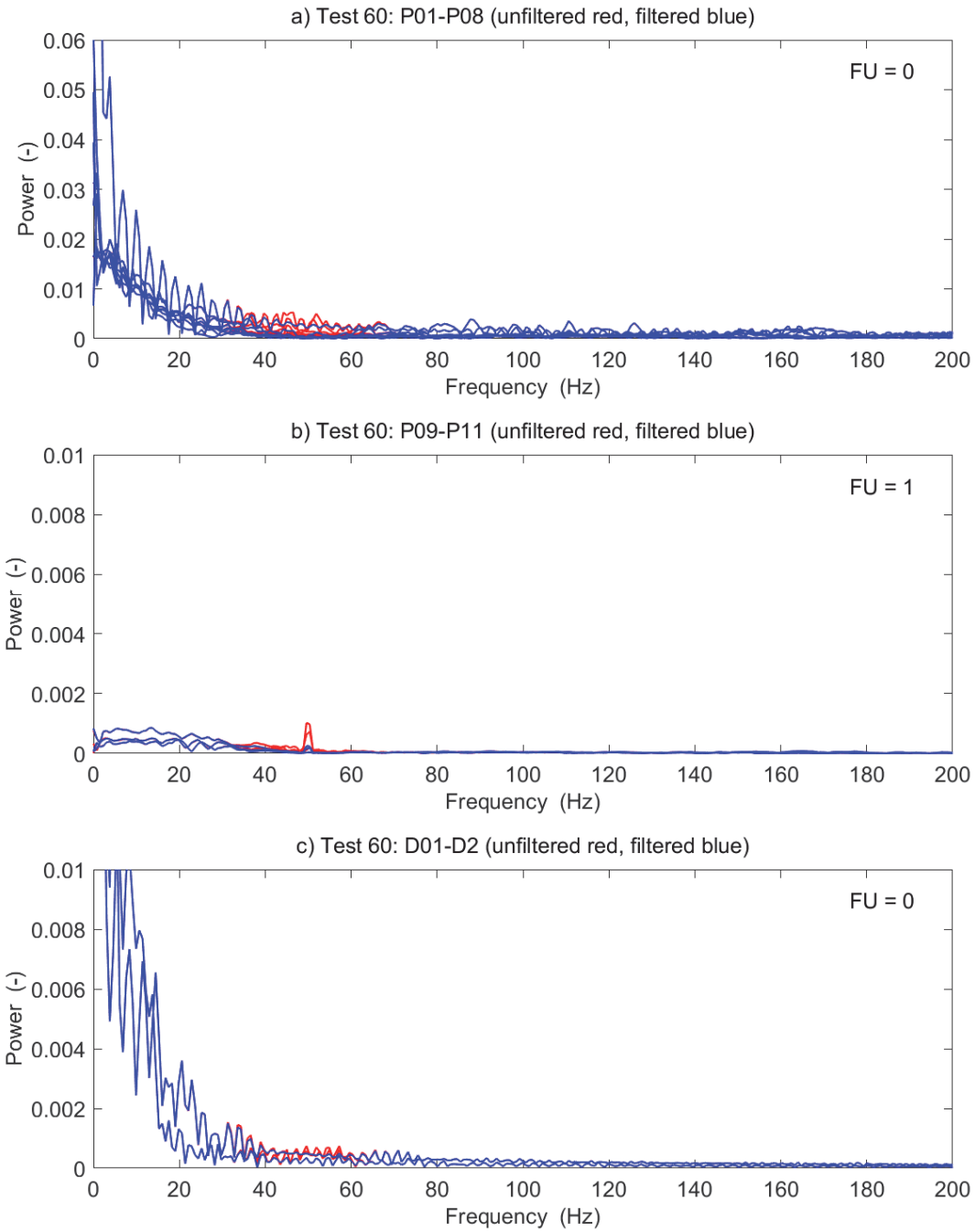

Figure 4: Power spectra from FFT analysis of pressure and displacement data for test 60.

Figure 5 summarises the filtered pressure-time histories for the internal pressure sensors (a) and the external blast gauges (b) for test no. 60 (example). The text included in the figures indicates the maximum values for the internal pressure (PM) and the external blast pressure (BM), as well as selected parameters from the test matrix: hydrogen concentration (H_2), vent area (A_v) and obstacle configuration (OC). The numerical values used for identifying OC were 1 for frame only (FO), 2 for bottle basket in inner position (B1), 3 for pipe rack in inner position (P1), 4 for pipe rack inner position and bottle basket outer position (P1B3), 5 for pipe rack in middle position (P2), and 6 for high congestion (HC). Skjold *et al.* (2018b) describe the experimental configurations, including the bottle basket (B) and pipe rack (P) obstacles. The squares and triangles indicate opening of panels and maximum pressures, respectively, and the vertical dash-dotted magenta, green and cyan lines indicate t_{stat}, t_{45} and t_{90}, respectively.

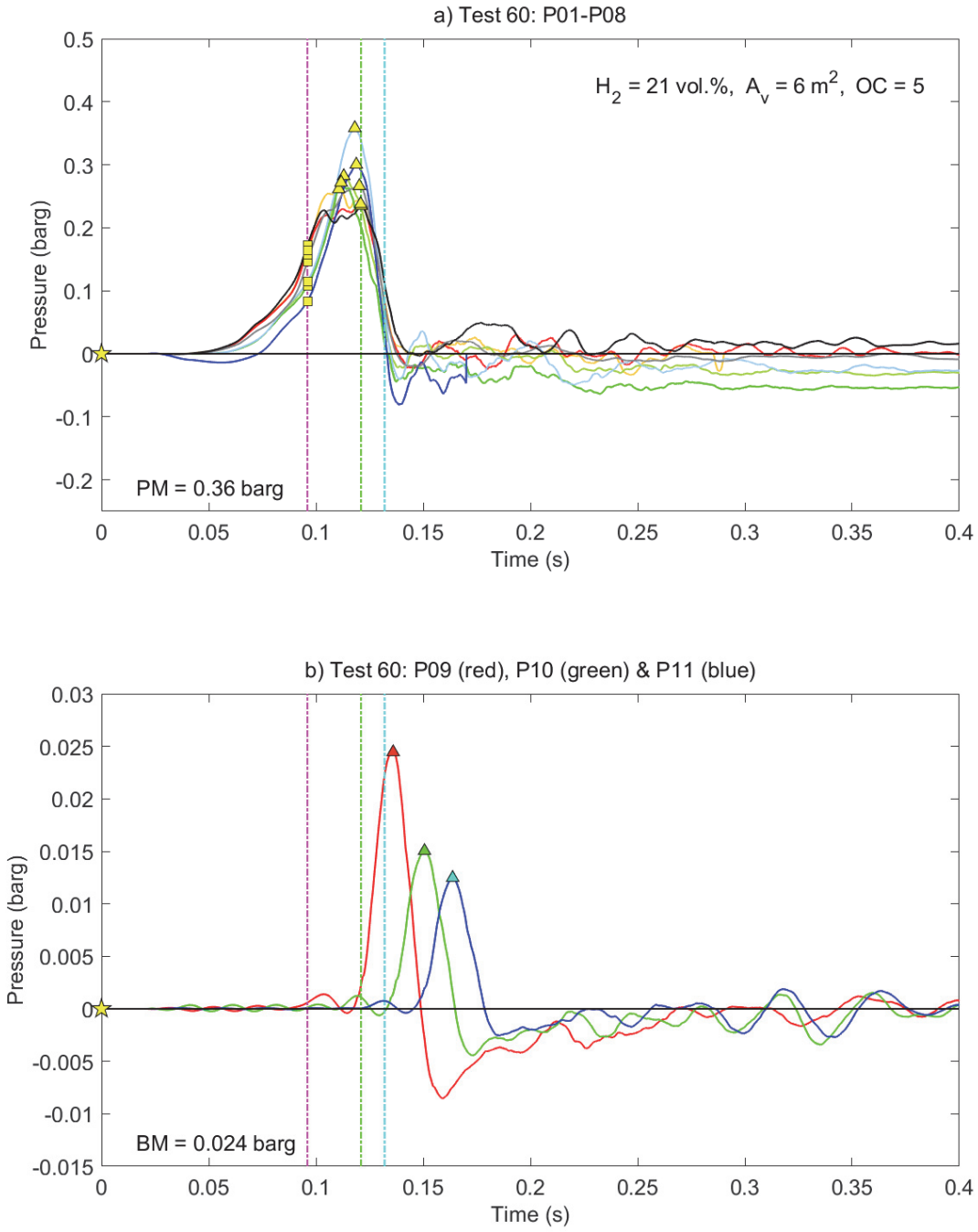

Figure 5: Summary of the filtered pressure-time histories for test no. 60.

Figure 6 summarises the filtered displacement-time histories (a) and the final permanent deformation measured by the two displacement sensors (b) for test no. 60 (example). The text in the figure indicates the values for the maximum displacement measured by sensors D01 and D02 (DM1 and DM2, respectively, also indicated by the red and light blue triangles), and the permanent deformation measured by D01 and D02 (DP1 and DP2, respectively). The vertical dash-dotted magenta, green and cyan lines in Figure 6 (a) indicate t_{stat}, t_{45} and t_{90}, respectively.

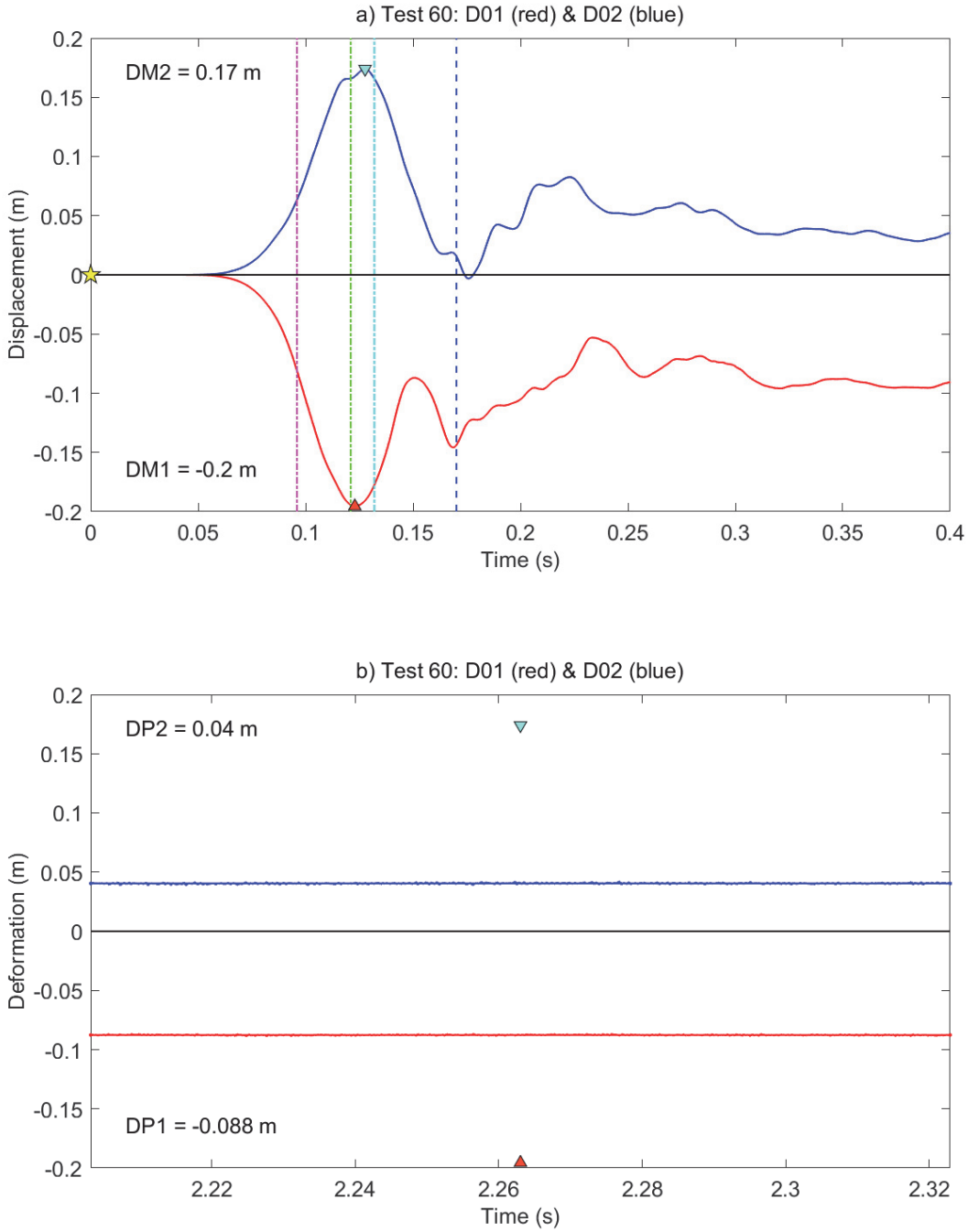

Figure 6: Summary of the filtered displacement-time histories for test no. 60.

Figure 7 (a) shows the maximum pressures P_m (yellow triangles for P01-P08, and red, green and cyan triangles for P09-P11, respectively) and the opening pressures P_{stat} for the venting devices (yellow squares) vs. distance from the back wall of the container to the sensors. The vertical dotted blue line (above) and the black line (below) indicate the location of the container doors (lines reversed for tests with venting through the doors). Figure 7 (b) shows pressure vs. impulse for the smoothed pressure-time histories measured by the internal pressure sensors P01-P08, from the time of ignition and up to end of the main pressure peak (indicated by the vertical blue dash-dotted lines in Figure 8). The triangles indicate the coordinates for maximum pressure and maximum impulse. Figure 7 (c) shows pressure vs. deflection for smoothed data measured by the internal pressure sensors P01-P08 and the deflection sensors D01 and D02. The dashed part of the lines represents the measurements beyond the main pressure peaks (defined above). The triangles indicate the coordinates for maximum pressure and maximum deflection.

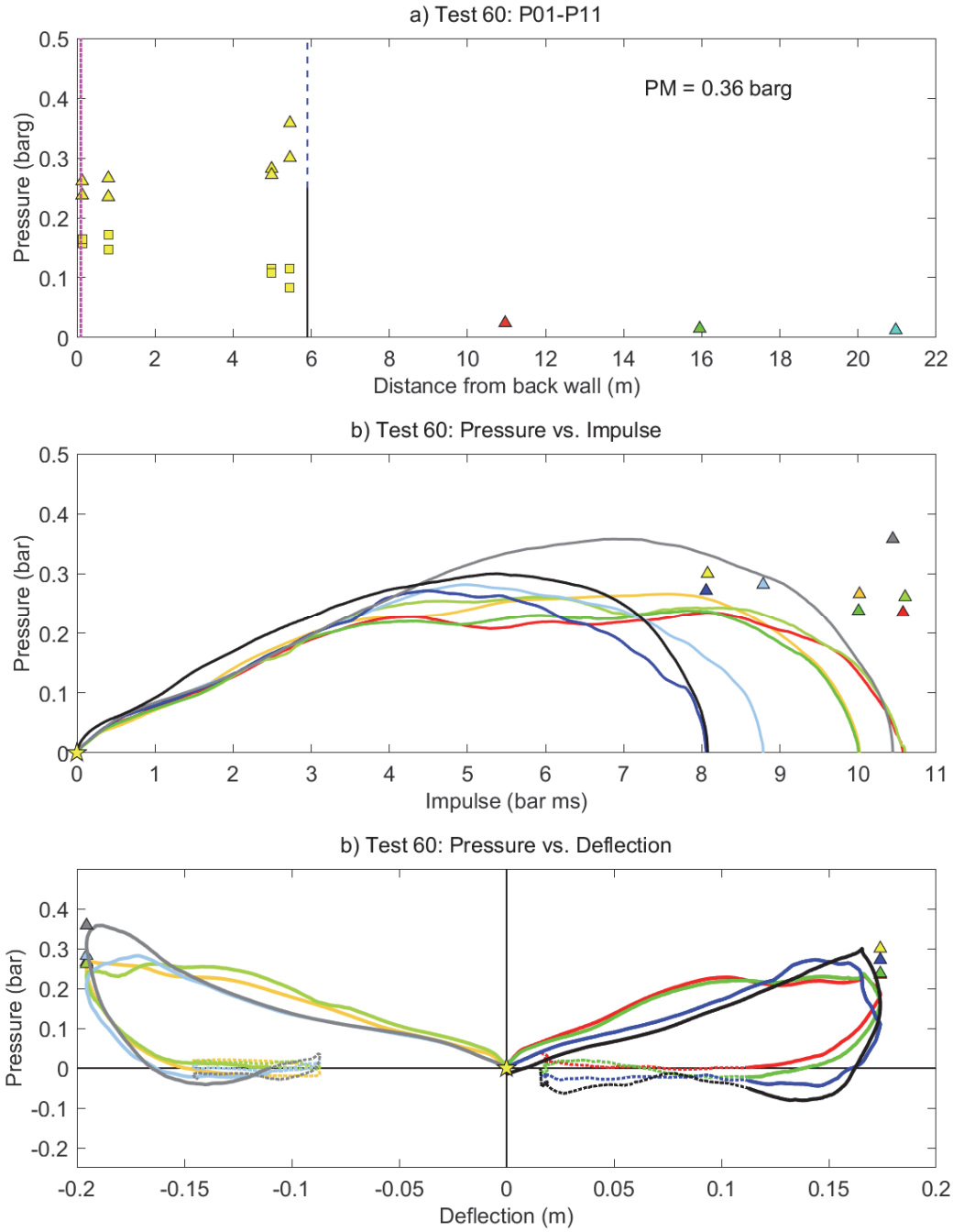

Figure 7: Summary of maximum pressure, impulse and structural response for test no. 60.

Figure 8 illustrates the integration of the filtered pressure-time histories measured by the internal pressure sensors P01-P09 for determining pressure impulse. The red and black lines are inherited from the plots in Figure 1 and Figure 2. The text in each plot indicates the calculated impulse (IM) in units bar milliseconds (bar-ms). The yellow triangles indicate the maximum pressures P_m for the smoothed pressure-time histories. The vertical dash-dotted magenta and blue lines indicate the opening time t_{stat} for the venting device and the time (manually defined) for ending the integration of the pressure-time histories (negative values neglected), respectively.

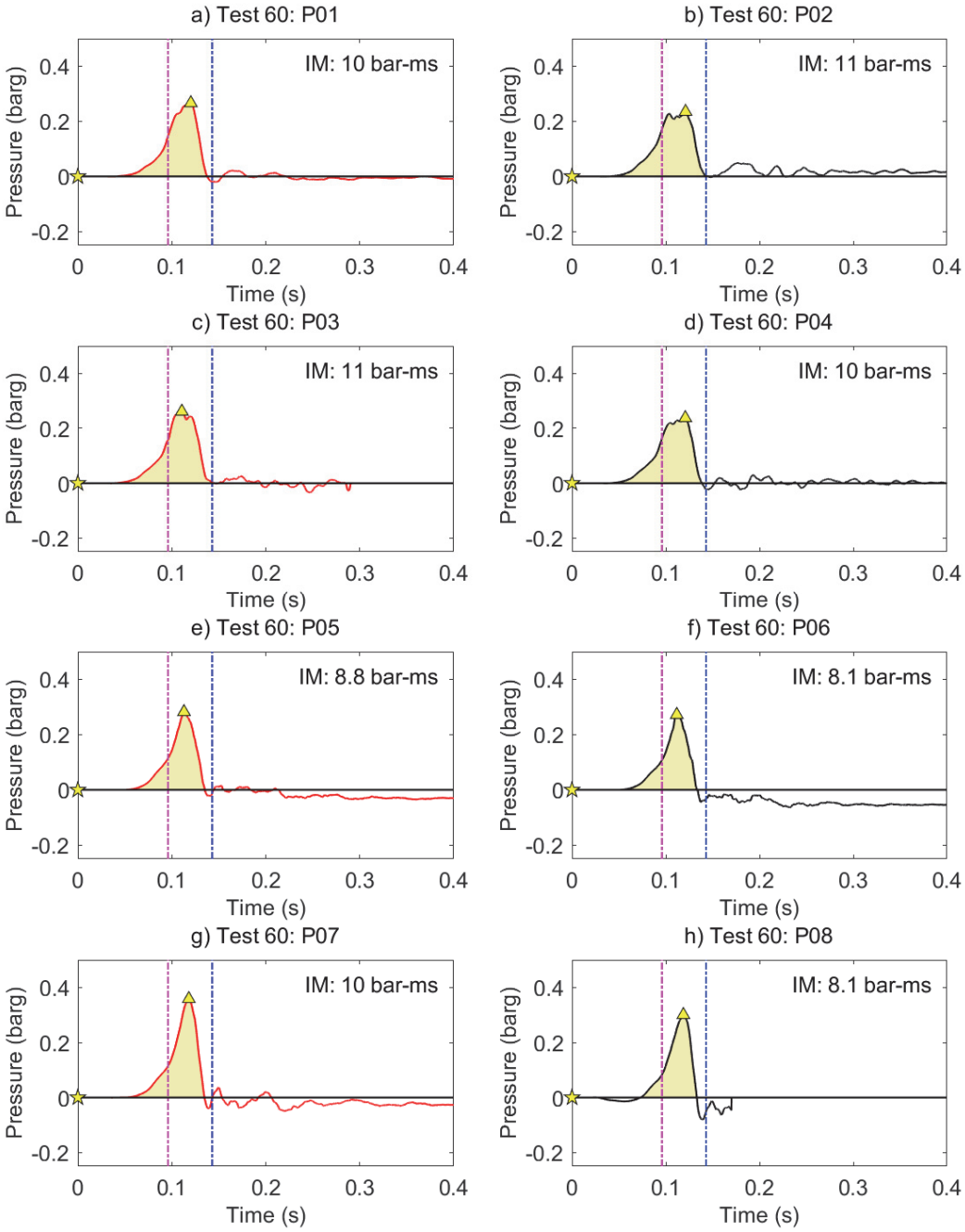

Figure 8: Integration of filtered pressure-time histories to determine impulse for test no. 60.

Figure 9 shows the derivative of the smoothed pressure-time histories measured by the internal pressure sensors P01-P08. The derivative is an output from the digital filter (Savitzky & Golay, 1964), and hence quite sensitive to the smoothing frequency used (Figure 10). The yellow squares indicate the opening pressures for the venting devices and the yellow circles indicate the maximum rate of pressure rise $(dP/dt)_m$. The vertical dash-dotted magenta and blue lines indicate the opening time t_{stat} for the venting device and the time for ending the numerical integration of the pressure-time histories, respectively.

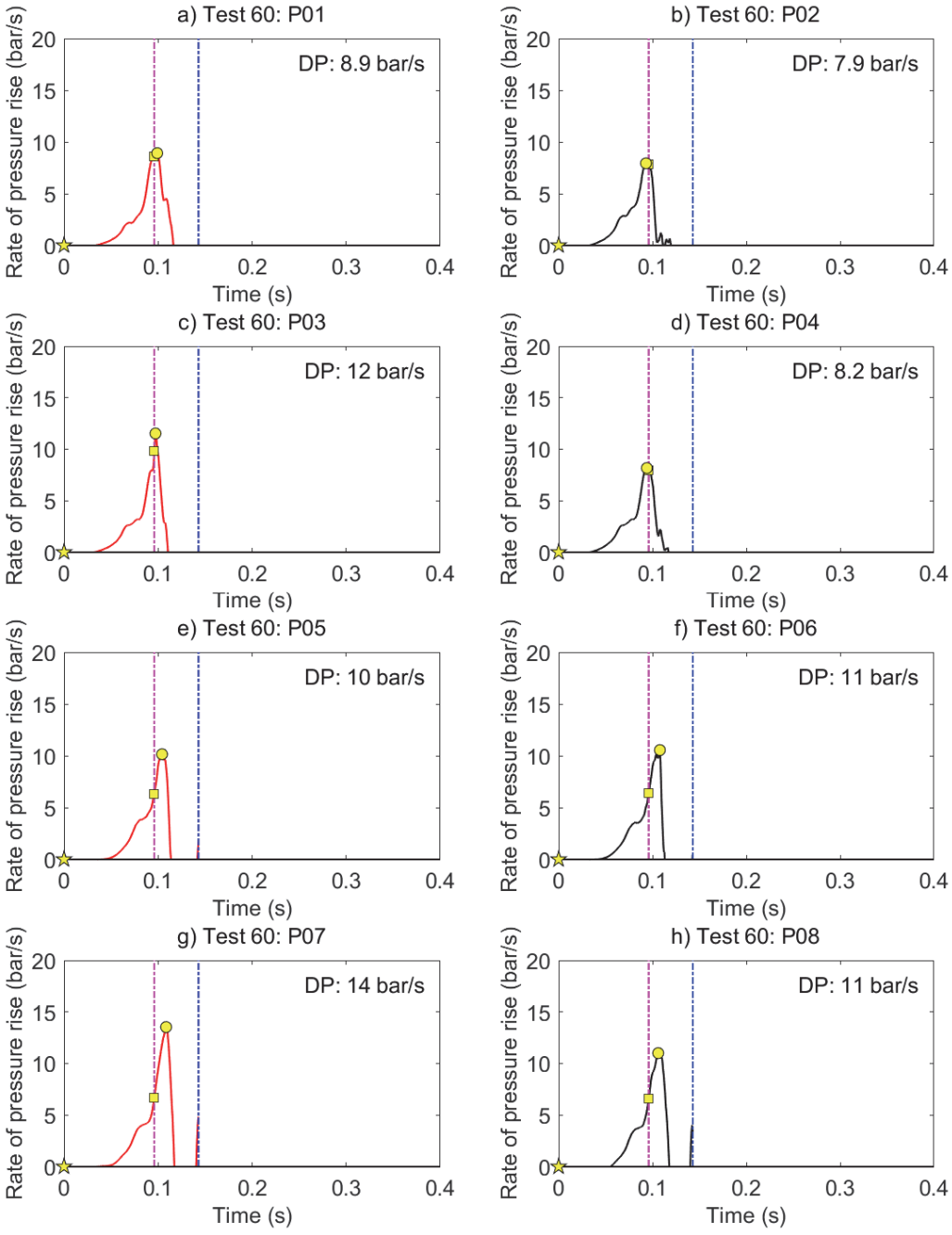

Figure 9: Maximum rate of pressure rise for filtered pressure-time histories from test no. 60.

Figure 10 illustrates the effect of varying the smoothing frequency of the digital filter (Savitzky & Golay, 1964) on the parameters average maximum pressure P_m, average maximum rate of pressure rise $(dP/dt)_m$, average impulse I_m and average maximum displacement D_m for the 66 vented deflagration tests. The error bars indicate the spread in results from the values derived from different sensors, from minimum to maximum values.

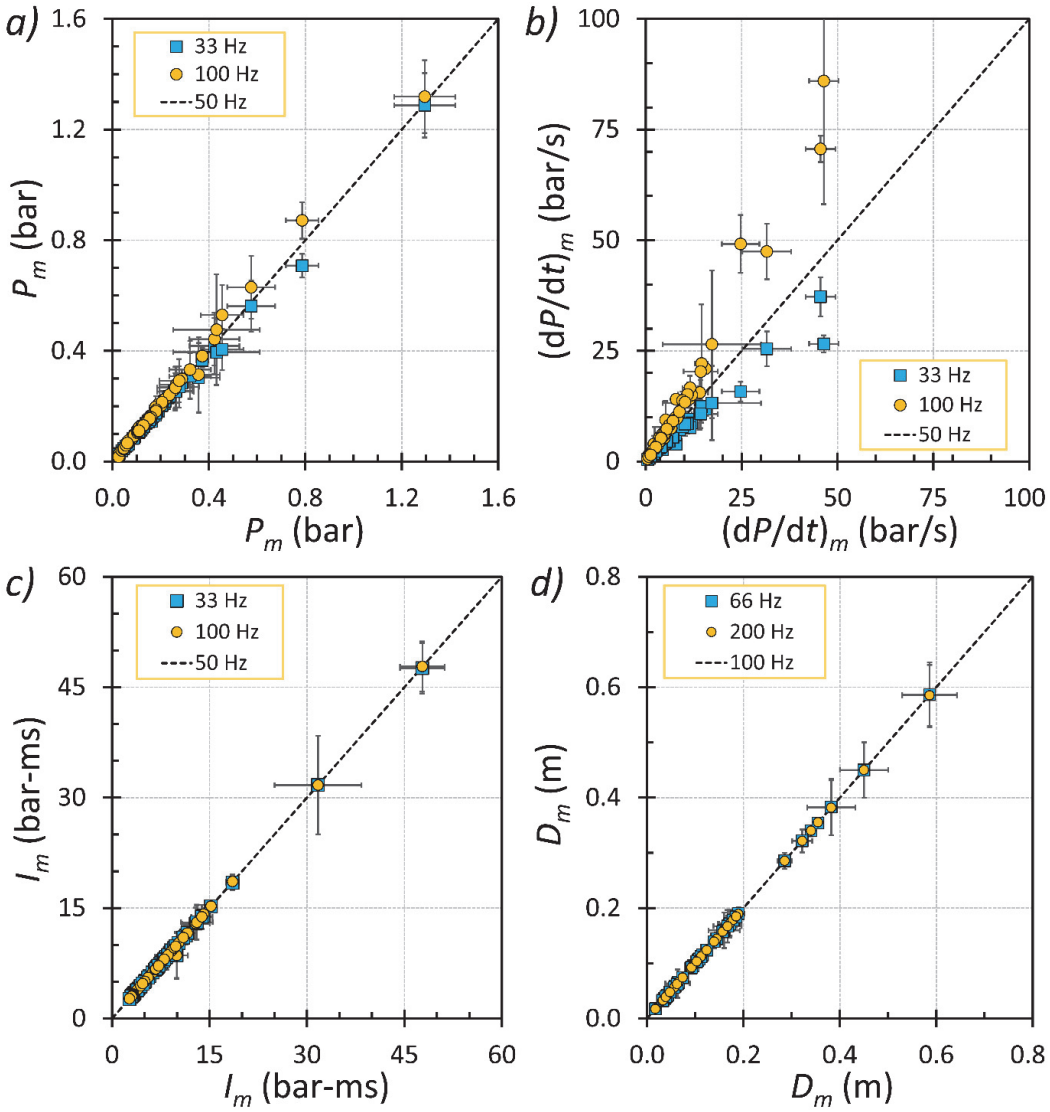

Figure 10: Effect of smoothing frequency on selected parameters.

4 Results

Table 2 summarises the maximum pressures recorded by the internal pressure sensors P01-P08 and the external blast gauges P09-P11, as well as the maximum deflection measured by the two laser displacement sensors D01-D02, for a smoothing frequency of 50 Hz. A significant fraction of the internal pressure measurements for the first 14-16 tests were discarded (NaN) due to significant drift and noise. The quality of the measurements was gradually improved by replacing the longest signal cables, i.e. the cables for sensors P03-P08 (Skjold *et al.*, 2018b).

Table 3 summarises the main results from the vented deflagration experiments with initially quiescent mixtures and venting through the doors (A_v = 5.56 m^2 and ignition position 'bc'): 14 tests vented through the doors, and one test (no. 70) with closed container.

Table 2: Maximum pressure and deflection for a smoothing frequency of 50 Hz (continues next page).

Test	P-01 (bar)	P-02 (bar)	P-03 (bar)	P-04 (bar)	P-05 (bar)	P-06 (bar)	P-07 (bar)	P-08 (bar)	P-09 (bar)	P-10 (bar)	P-11 (bar)	D-01 (m)	D-02 (m)
1	0.03	0.03	NaN	NaN	NaN	NaN	NaN	NaN	0.01	0.00	0.00	0.02	0.02
2	0.02	0.03	NaN	NaN	NaN	NaN	NaN	NaN	0.01	0.00	0.00	0.04	0.04
3	0.07	0.07	NaN	NaN	NaN	NaN	NaN	NaN	0.03	0.01	0.01	0.11	0.09
4	0.06	0.06	NaN	NaN	NaN	NaN	NaN	NaN	0.01	0.01	0.00	0.07	0.05
5	0.04	0.04	NaN	NaN	NaN	NaN	NaN	NaN	NaN	0.00	0.00	0.02	0.01
6	0.05	0.05	NaN	NaN	NaN	NaN	NaN	NaN	0.01	0.02	0.00	0.04	0.03
7	0.20	0.18	NaN	NaN	NaN	NaN	NaN	NaN	0.08	0.05	0.03	0.20	0.18
8	0.40	0.35	NaN	NaN	NaN	NaN	NaN	NaN	0.15	0.09	0.05	0.50	0.40
9	1.42	1.17	NaN	NaN	NaN	NaN	NaN	NaN	0.25	0.14	0.10	NaN	NaN
10	0.13	0.13	0.12	0.12	NaN	NaN	NaN	NaN	0.05	0.03	0.02	NaN	NaN
11	0.05	0.05	0.05	0.04	NaN	NaN	NaN	NaN	0.01	0.01	0.00	0.04	0.04
12	0.12	0.12	0.11	0.11	NaN	NaN	NaN	NaN	0.04	0.02	0.02	0.18	0.18
13	0.25	0.28	0.25	0.24	NaN	NaN	NaN	NaN	0.14	0.08	0.05	0.35	0.33
14	0.85	0.85	0.71	0.73	NaN	NaN	NaN	NaN	0.18	0.09	0.06	0.27	0.30
15	0.17	0.17	NaN	0.17	0.18	0.19	0.19	0.18	0.03	0.06	0.01	0.30	0.34
16	0.16	0.16	NaN	NaN	NaN	NaN	0.17	NaN	0.03	0.11	0.02	0.04	0.07
17	0.10	0.11	0.10	0.10	0.11	NaN	0.12	0.11	0.03	0.04	0.01	0.05	0.07
18	0.21	0.22	0.20	0.21	0.23	NaN	0.21	0.22	0.03	0.07	0.01	0.13	0.19
19	0.12	0.12	0.11	0.11	0.12	0.12	0.13	0.13	0.03	0.05	0.01	0.04	0.09
20	0.28	0.29	NaN	0.27	0.31	0.27	0.30	0.28	0.03	0.10	0.01	0.15	0.20
21	0.09	0.08	0.09	0.09	0.10	0.10	0.10	0.10	0.03	0.05	0.02	0.03	0.05
22	0.10	0.12	0.11	0.11	0.12	0.12	0.12	0.10	0.03	0.05	0.01	0.07	0.06
23	0.13	0.17	0.15	0.15	0.16	0.14	0.16	0.15	0.03	0.06	0.02	0.10	0.08
24	0.10	0.13	0.11	0.12	0.14	0.12	0.14	NaN	0.02	0.05	0.01	0.07	0.06
25	0.12	0.13	0.12	0.13	0.14	0.14	0.14	NaN	0.03	0.07	0.01	0.06	0.06
26	0.18	0.19	0.18	0.19	NaN	0.18	0.20	0.18	0.04	0.09	0.02	0.10	0.10
27	0.22	0.24	0.23	0.23	NaN	0.21	0.25	0.22	0.03	0.00	0.01	0.16	0.15
28	0.34	0.45	0.31	0.33	NaN	NaN	0.37	0.33	0.03	NaN	0.02	0.19	0.15
29	NaN	NaN	NaN	NaN	NaN	NaN	0.21	NaN	0.03	0.07	0.01	0.19	0.15
30	0.18	NaN	0.17	0.15	0.20	0.20	0.21	NaN	0.02	0.07	0.01	NaN	NaN
31	0.22	0.22	0.20	0.17	0.23	0.25	0.24	NaN	0.02	0.06	0.01	0.13	0.16
32	0.19	0.20	0.18	NaN	0.22	0.21	0.21	NaN	0.02	0.07	0.01	0.10	0.12
33	0.23	0.24	0.21	NaN	0.25	0.24	0.25	NaN	0.02	0.05	0.01	0.10	0.12
34	0.34	0.39	0.42	0.45	0.50	0.53	NaN	0.33	0.06	NaN	0.03	NaN	NaN
35	0.09	0.06	0.13	0.13	0.12	0.12	0.13	NaN	0.02	NaN	0.01	NaN	NaN
36	0.16	0.18	0.15	0.19	NaN	NaN	0.20	0.19	0.03	0.02	0.01	0.11	0.10
37	0.20	0.22	0.22	0.23	0.16	0.17	0.23	0.22	0.03	0.02	0.01	0.12	0.11
38	0.11	0.14	0.12	0.15	0.15	0.15	0.15	0.14	0.02	0.01	0.01	NaN	NaN
44	0.24	NaN	0.29	0.29	0.36	0.35	0.41	NaN	0.03	0.02	0.01	0.15	0.16
45	0.09	0.08	0.09	0.09	0.08	0.08	0.08	0.08	0.01	0.00	0.00	0.04	0.04
46	0.16	0.13	0.18	0.18	0.16	0.16	0.18	NaN	0.01	0.01	0.01	0.10	0.12
47	0.15	NaN	0.19	0.19	0.19	0.18	NaN	0.19	0.01	0.01	0.01	0.15	0.13
48	0.14	NaN	0.17	0.17	0.17	0.17	NaN	NaN	0.01	0.01	0.01	0.13	0.12

Test	P-01 (bar)	P-02 (bar)	P-03 (bar)	P-04 (bar)	P-05 (bar)	P-06 (bar)	P-07 (bar)	P-08 (bar)	P-09 (bar)	P-10 (bar)	P-11 (bar)	D-01 (m)	D-02 (m)
49	0.14	NaN	0.18	0.18	0.18	0.17	NaN	0.16	0.02	0.01	0.01	0.09	0.09
50	0.15	NaN	0.18	0.19	0.19	0.19	NaN	0.18	0.01	0.01	0.00	0.13	0.12
51	0.06	NaN	0.06	0.06	0.05	0.05	NaN	NaN	0.01	0.01	0.01	0.04	0.04
52	0.06	NaN	0.07	0.07	0.06	0.07	NaN	NaN	0.02	0.01	0.01	0.03	0.03
53	0.10	NaN	0.11	0.11	0.07	0.07	NaN	0.07	0.01	0.01	0.01	0.06	0.06
54	0.06	NaN	0.08	0.08	0.05	0.05	NaN	NaN	0.02	0.01	0.01	0.04	0.04
55	0.13	NaN	0.16	0.16	0.14	0.14	NaN	0.15	0.01	0.01	0.01	0.09	0.09
56	0.12	NaN	0.16	0.16	0.15	0.14	NaN	0.15	0.01	0.01	0.01	0.09	0.09
57	0.18	NaN	0.24	0.25	0.29	0.28	NaN	0.33	0.02	0.01	0.01	0.18	0.18
59	0.22	0.24	0.24	0.24	0.27	0.27	0.34	NaN	0.02	0.01	0.01	0.20	0.14
60	0.27	0.23	0.26	0.24	0.28	0.27	0.36	0.30	0.02	0.02	0.01	0.20	0.17
61	0.36	NaN	0.39	0.41	0.33	0.34	0.61	0.58	0.04	0.02	0.04	0.43	0.33
62	0.13	0.16	0.15	0.15	0.14	0.13	0.15	0.13	0.01	0.00	0.00	0.07	0.06
63	0.13	0.16	0.16	0.16	0.16	0.16	0.17	NaN	0.01	0.00	0.00	0.10	0.08
64	0.13	0.15	0.15	0.15	0.15	0.14	0.16	NaN	0.01	0.00	0.00	0.10	0.09
65	0.13	0.16	0.16	0.16	0.16	0.15	0.16	0.15	0.01	0.01	0.01	0.11	0.10
66	0.10	0.11	0.10	0.10	0.10	0.10	0.11	0.10	0.01	0.00	0.00	0.07	0.06
67	0.10	0.11	0.11	0.11	0.11	0.10	0.11	0.10	NaN	0.00	0.00	NaN	0.06
68	0.12	0.13	0.13	0.13	0.13	0.13	0.14	0.12	0.01	0.01	0.00	0.08	0.07
69	0.53	0.61	0.66	0.67	0.49	0.48	0.61	0.55	0.09	0.05	0.04	0.53	0.64
70	0.31	0.30	0.34	0.36	NaN	NaN	0.36	0.34	NaN	NaN	NaN	0.19	0.20
71	NaN	0.11	NaN	0.11	0.11	0.11	0.12	0.11	0.00	0.00	0.00	0.05	0.04
72	NaN	0.54	0.53	0.52	0.36	0.37	0.44	0.42	0.03	0.02	0.01	0.35	0.36

Table 3: Summary of experiments with initially quiescent mixtures and venting through the doors.

Test	C_{H2} (vol.%)	A_v (m^2)	Vent	Ign.	Obst.	Atm.	P_{max} (bar)	P_m (bar)	D_m (m)	D_p (m)	$(dP/dt)_m$ (bar/s)	I_m (bar-ms)
1 [a]	15	5.56	D	bc	FO	HQ	0.030	0.029	0.018	0.000	0.49	3.5
2 [a]	15	5.56	D	bc	FO	HQ	0.027	0.026	0.042	0.001	0.46	3.4
5 [a]	15	5.56	D	bc	FO	HQ	0.039	0.039	0.017	0.000	0.97	3.3
3 [a]	15	5.56	D	bc	B1	HQ	0.068	0.067	0.096	0.011	1.2	5.8
4 [a]	15	5.56	D	bc	B1	HQ	0.057	0.056	0.063	0.001	1.3	6.2
6 [a]	15	5.56	D	bc	B1	HQ	0.046	0.045	0.032	0.002	0.96	3.8
10	18	5.56	D	bc	B1	HQ	0.132	0.127	—	—	3.7	7.4
7	21	5.56	D	bc	B1	HQ	0.199	0.191	0.190	0.031	8.5	8.6
8	24	5.56	D	bc	B1	HQ	0.398	0.373	0.450	—	15.6	14.1
11	15	5.56	D	bc	P1	HQ	0.050	0.047	0.040	0.002	1.34	3.2
12	18	5.56	D	bc	P1	HQ	0.119	0.115	0.179	0.020	5.3	7.1
13	21	5.56	D	bc	P1	HQ	0.277	0.255	0.340	0.031	11.2	11.4
14 [b]	21	5.56[b]	D	bc	P1B3	HQ	0.854	0.787	0.285	0.103	46.4	18.6
9 [c]	24	5.56[c]	C	bc	B1	HQ	1.422	1.295	—	—	45.6	47.8
70 [d]	12	~ 0[d]	S	fc	FO	HQ	0.358	0.335	0.193	0.065	0.99	397

[a] The first HySEA blind-prediction benchmark exercise involved tests 1-6 (Skjold *et al.*, 2018c).
[b] The bottle basket partly blocked the vent opening in test 14, implying that the actual vent area was less than 5.56 m^2.
[c] The container doors were initially closed in test 09, but opened during the test.
[d] The container doors were closed in test 70, but some leakage occurred.

Table 4 summarises the main results from the 27 vented deflagration experiments with initially quiescent mixtures and venting through the roof.

Table 4: Summary of experiments with initially quiescent mixtures and venting through the roof.

Test	C_{H2} (vol.%)	A_v (m^2)	Vent	Ign.	Obst.	Atm.	P_{max} (bar)	P_m (bar)	D_m (m)	D_p (m)	$(dP/dt)_m$ (bar/s)	I_m (bar-ms)
45	21	6.0	O	bu	FO	HQ	0.095	0.084	0.037	0.002	2.5	3.2
25	21	4.0	O	fc	FO	HQ	0.143	0.131	0.056	0.003	4.3	5.6
21	21	6.0	O	fc	FO	HQ	0.101	0.093	0.043	0.004	3.6	4.3
16	21	8.0	O	fc	FO	HQ	0.171	0.163	0.056	0.007	7.9	7.0
24	21	4.0	O	fc	P2	HQ	0.140	0.123	0.065	0.003	4.4	5.1
29	24	4.0	O	fc	P2	HQ	0.215	0.215	0.172	0.069	12.0	15.2
22	21	6.0	O	fc	P2	HQ	0.118	0.112	0.065	0.012	5.2	3.9
23	24	6.0	O	fc	P2	HQ	0.165	0.150	0.091	0.026	7.8	4.4
17	21	8.0	O	fc	P2	HQ	0.116	0.110	0.058	0.006	4.8	3.8
19	24	8.0	O	fc	P2	HQ	0.132	0.119	0.063	0.014	6.1	4.1
34	42	8.0	O	fc	P2	HQ	0.526	0.423	—	—	14.5	31.7
46	21	6.0	P	bu	FO	HQ	0.182	0.163	0.112	0.019	4.6	6.6
47	21	6.0	P	bu	FO	HQ	0.192	0.182	0.139	0.023	5.1	6.9
32	21	4.0	P	fc	FO	HQ	0.216	0.202	0.112	0.012	4.9	10.2
26	21	6.0	P	fc	FO	HQ	0.197	0.186	0.103	0.007	4.7	9.5
15	21	8.0	P	fc	FO	HQ	0.188	0.178	0.322	0.101	4.5	9.7
71	12	6.0	P	fc	HC	HQ	0.117	0.110	0.048	0.002	1.3	11.0
72	15	6.0	P	fc	HC	HQ	0.543	0.455	0.355	0.278	24.7	13.8
48	21	6.0	P	bu	P2	HQ	0.175	0.166	0.124	0.013	4.5	7.0
33	21	4.0	P	fc	P2	HQ	0.248	0.236	0.106	0.004	6.6	9.2
27	21	6.0	P	fc	P2	HQ	0.248	0.230	0.158	0.042	8.1	9.0
31	21	6.0	P	fc	P2	HQ	0.245	0.219	0.145	0.016	6.7	8.2
28	24	6.0	P	fc	P2	HQ	0.446	0.309	0.168	0.081	12.3	8.6
18	21	8.0	P	fc	P2	HQ	0.234	0.214	0.160	0.040	8.5	7.6
30	21	8.0	P	fc	P2	HQ	0.210	0.183	—	—	6.2	7.1
20	24	8.0	P	fc	P2	HQ	0.314	0.288	0.171	0.083	11.4	8.9
69	42	8.0	P	fc	P2	HQ	0.675	0.575	0.586	0.476	31.6	13.0

Error! Not a valid bookmark self-reference. summarises the main results from the 17 tests with stratified mixtures and venting through the roof.

Table 5: Summary of experiments with stratified mixtures and venting through the roof.

Test	C_{H2} (vol.%)	A_v (m²)	Vent	Ign.	Obst.	Atm.	P_{max} (bar)	P_m (bar)	D_m (m)	D_p (m)	$(dP/dt)_m$ (bar/s)	I_m (bar-ms)
54	18	6.0	O	bu	FO	SJ	0.076	0.062	0.039	0.002	1.974	2.677
51	18	6.0	O	bu	P2	SJ	0.061	0.056	0.037	0.001	2.313	2.957
53	18	6.0	O	bu	FO	SD	0.109	0.089	0.063	0.000	2.768	3.002
52	18	6.0	O	bu	P2	SD	0.071	0.067	0.033	0.000	2.117	3.094
65	15	6.0	P	bu	FO	SJ	0.162	0.155	0.103	0.000	3.949	6.740
55	18	6.0	P	bu	FO	SJ	0.159	0.147	0.093	0.009	3.530	6.641
57 [a]	21	6.0	P	bu	FO	SJ	0.332	0.264	0.178	0.042	10.888	7.867
59 [a]	21	6.0	P	bu	FO	SJ	0.337	0.261	0.167	0.030	9.562	8.044
64	15	6.0	P	bu	FO	SD	0.159	0.147	0.092	0.000	3.660	6.849
56	18	6.0	P	bu	FO	SD	0.163	0.149	0.091	0.008	3.538	6.838
44	21	6.0	P	bu	FO	SD	0.408	0.322	0.157	0.071	14.324	8.627
62	15	6.0	P	bu	P2	SJ	0.156	0.141	0.065	0.009	3.028	6.744
50	18	6.0	P	bu	P2	SJ	0.193	0.181	0.124	0.006	5.469	6.972
60 [a]	21	6.0	P	bu	P2	SJ	0.358	0.277	0.185	0.064	10.227	9.570
61 [a]	21	6.0	P	bu	P2	SJ	0.611	0.432	0.382	0.263	17.251	11.606
63 [b]	15	5.0[b]	P	bu	P2	SD	0.173	0.160	0.091	0.010	4.057	6.941
49	18	6.0	P	bu	P2	SD	0.184	0.169	0.092	0.010	4.811	6.704

[a] The second HySEA blind-prediction benchmark exercise involved tests 57, 59, 60 and 61 (Skjold *et al.*, 2018d).

[b] Only five of the six vent panels installed on the container opened in test 63.

Error! Not a valid bookmark self-reference. summarises the main results from seven tests with initial turbulence generated by either a fan (TF) or a transient jet (TJ), vented through the roof.

Table 6: Summary of experiments with initially turbulent mixtures and venting through the roof.

Test	C_{H2} (vol.%)	A_v (m²)	Vent	Ign.	Obst.	Atm.	P_{max} (bar)	P_m (bar)	D_m (m)	D_p (m)	$(dP/dt)_m$ (bar/s)	I_m (bar-ms)
35	18	8.0	O	fc	P2	TF	0.135	0.112	—	—	6.086	3.294
36	21	8.0	O	fc	P2	TF	0.205	0.179	0.108	0.031	11.550	5.020
38	21	4.0	O	fc	P2	TF	0.152	0.138	—	—	7.076	4.722
37	21	6.0	O	fc	P2	TF	0.230	0.206	0.115	0.013	8.764	8.361
66	15	4.0[a]	P	bu	FO	TJ	0.107	0.104	0.065	0.006	0.798	12.894
67 [a]	18	4.0[a]	P	bu	FO	TJ	0.112	0.107	0.062	0.005	1.226	9.801
68 [a]	21	6.0	P	bu	FO	TJ	0.137	0.128	0.074	0.005	2.624	7.166

[a] Only four of the six vent panels installed on the container opened in tests 66 and 67.

Table 7 summarises the time t_{stat} and the corresponding pressure P_{stat} when the venting devices in the 66 vented deflagration tests start to open. The table also includes the times t_{45}, t_{90} and t_{180} relative to t_{stat} when the panels had opened 45º, 90º and 180º, respectively. The times for the opening of the panels were estimated from high-speed video recordings.

Table 7: Opening of venting devices (continues on next page).

Test	t_{stat} (s)	P_{stat} (bar)	t_{45} (s)	t_{90} (s)	t_{180} (s)
1	0.190	0.017	—	—	—
2	0.192	0.026	—	—	—
3	0.187	0.037	—	—	—
4	0.213	0.054	—	—	—
5	0.190	0.008	—	—	—
6	0.242	0.027	—	—	—
7	0.091	0.045	—	—	—
8	0.058	0.055	—	—	—
9	0.095	0.990	0.011	0.026	—
10	0.123	0.042	—	—	—
11	0.271	0.047	—	—	—
12	0.117	0.025	—	—	—
13	0.084	0.085	—	—	—
14	0.090	0.173	—	—	—
15	0.112	0.178	0.023	0.041	0.081
16	0.098	0.103	—	—	—
17	0.099	0.079	—	—	—
18	0.099	0.181	0.021	0.035	0.057
19	0.093	0.046	—	—	—
20	0.096	0.150	0.020	0.031	0.054
21	0.082	0.059	—	—	—
22	0.090	0.084	—	—	—
23	0.074	0.037	—	—	—
24	0.098	0.060	—	—	—
25	0.081	0.039	—	—	—
26	0.102	0.148	0.025	0.038	0.062
27	0.088	0.136	0.025	0.036	0.061
28	0.072	0.128	0.023	0.032	0.053
29	0.066	0.077	—	—	—
30	0.146	0.129	0.025	0.037	0.064
31	0.143	0.119	0.028	0.039	0.064
32	0.123	0.141	0.026	0.037	0.061
33	0.279	0.135	0.024	0.038	0.061
34	0.045	0.034	—	—	—
35	0.069	0.022	—	—	—
36	0.068	0.085	—	—	—
37	0.085	0.125	—	—	—
38	0.079	0.072	—	—	—
44	0.108	0.098	0.025	0.038	0.058
45	0.100	0.040	—	—	—
46	0.107	0.106	0.032	0.046	0.078
47	0.121	0.125	0.027	0.043	0.072
48	0.112	0.115	0.029	0.046	0.076
49	0.124	0.140	0.028	0.042	0.070

Test	t_{stat} (s)	P_{stat} (bar)	t_{45} (s)	t_{90} (s)	t_{180} (s)
50	0.107	0.091	0.035	0.052	0.082
51	0.106	0.051	—	—	—
52	0.090	0.026	—	—	—
53	0.100	0.065	—	—	—
54	0.090	0.045	—	—	—
55	0.139	0.118	0.032	0.052	0.092
56	0.135	0.122	0.029	0.048	0.083
57	0.082	0.142	0.022	0.035	0.059
59	0.083	0.123	0.026	0.038	0.061
60	0.096	0.133	0.025	0.036	0.058
61	0.076	0.115	0.025	0.034	0.05
62	0.143	0.113	0.033	0.053	0.092
63	0.147	0.143	0.051	0.083	0.174
64	0.141	0.114	0.036	0.058	0.101
65	0.125	0.112	0.034	0.051	0.088
66	0.412	0.098	0.042	0.071	0.127
67	0.298	0.103	0.054	0.088	0.161
68	0.173	0.101	0.04	0.063	0.106
69	0.062	0.294	—	—	—
70	3.999	—	—	—	—
71	0.547	0.104	0.044	0.086	0.164
72	0.241	0.127	0.023	0.032	0.051

Figure 11 summarises the results for the maximum reduced explosion pressure for 65 of the 66 vented deflagration tests. The results from test no. 70 is not included since this test was performed to study structural response under quasi-static loading conditions ($A_v \approx 0$ m^2).

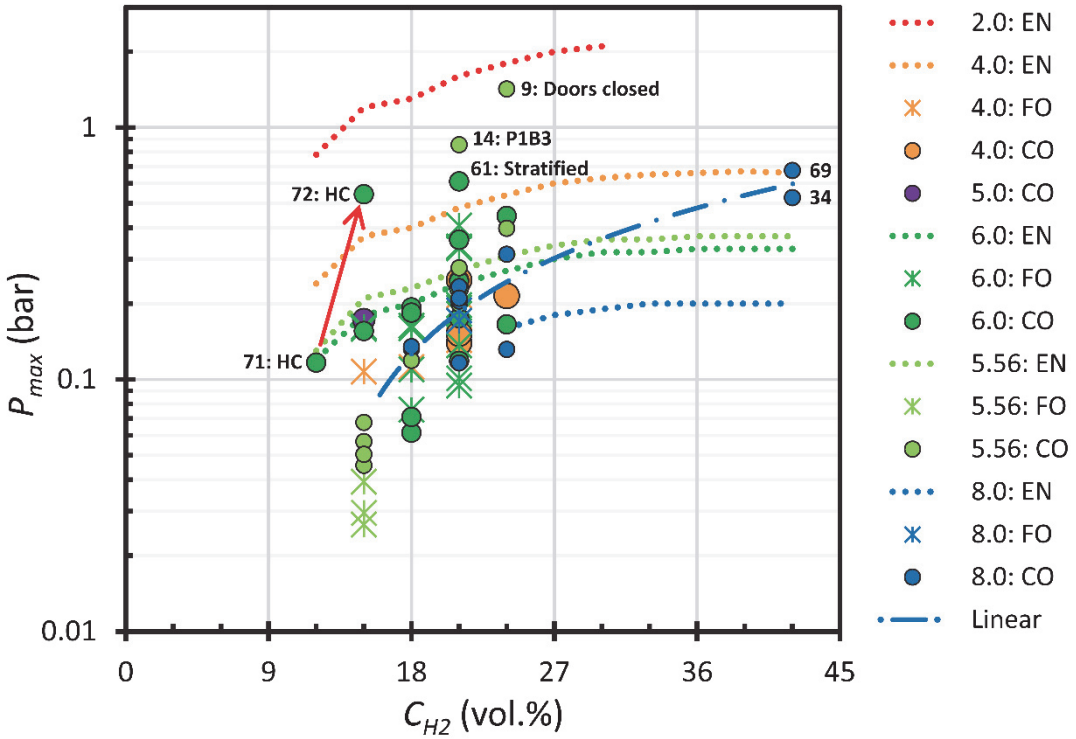

Figure 11: Summary of maximum reduced explosion pressures.

5 Discussion

For the sake of brevity, the data series represented in Figure 11 do not distinguish between tests with different types of venting devices, nor between tests with homogeneous or non-homogeneous mixtures and tests with or without initial turbulence. This representation results in a plot with significant scatter, typically an order of magnitude variation in the maximum reduced explosion pressures for a given fuel concentration. Skjold *et al.* (2018b) present plots of more diversified data series from the same experiments.

Figure 11 includes predictions by the empirical correlations in the European standard for gas explosion venting devices (EN 14994, 2007) for certain vent areas (dotted lines). However, the standard assumes worst-case conditions for homogeneous and initially quiescent mixtures in empty enclosures (i.e. maximum flame length and most reactive mixture), and the correlations in the standard are only applicable for flammable atmospheres with gas explosion constants $K_G \leq 550$ bar m s^{-1}. This corresponds to the reactivity of hydrogen-air mixtures with concentrations in the range 22-28 % hydrogen (Holtappels, 2006). As such, the EN standard is not strictly applicable for hydrogen. To circumvent this, the model predictions indicated in Figure 11 were obtained with the commercial software package WinVent 4.0 using published values for the maximum rate of pressure rise and the maximum explosion pressure measured in a 6-litre vessel (Holtappels, 2006). This approach implies significant uncertainty, since flame wrinkling and other instabilities cause experimentally determined K_G values to vary significantly with the volume and shape of the test vessel (Holtappels, 2006). Furthermore, since the EN standard assumes a static opening pressure P_{stat} of 0.10 bar, the correlations over-predict the reduced explosion pressure for tests with low reactivity mixtures and vent openings covered by polyethylene film (Skjold *et al.*, 2018b). It is nevertheless of interest to compare the overall trends in the model predictions to the results obtained in the HySEA experiments.

Figure 11 highlights results from selected tests that demonstrate some of the limitations associated with the empirical correlations in EN 14994 (2007), as well as most other empirical or semi-empirical models for vented deflagrations:

1. The dramatic increase in pressure for the relatively modest increase in fuel concentration for the two high-congestion (HC) cases, from 12 to 15 vol.% H_2 for tests 71 and 72 (red arrow), illustrates the strong effect congestion can have on flame acceleration and pressure build-up in vented deflagrations. It is not straightforward to include the effect of congestion in empirical or semi-empirical correlations. Furthermore, under certain conditions local congestion and/or confinement inside an enclosure may result in deflagration-to-detonation transition (DDT), and hence no mitigating effect of any explosion venting device.
2. Hydrogen has low molecular weight, and loss of containment of gaseous hydrogen in confined spaces will typically result in buoyant releases and stratified fuel-air clouds (Skjold *et al.*, 2018d). The high pressures obtained for stratified mixtures (e.g. test no. 61 from Table 5), compared to lean homogeneous mixtures containing the same mass of fuel (e.g. tests no. 27, 31 and 48 from Table 4), imply that models for vented hydrogen deflagrations should account for the effect of stratification. Although such models exist (Makarov *et al.*, 2018), it is not straightforward to verify and validate the models, as well as to apply the results in practical risk assessments for enclosures with spatial scales and levels of congestion representative of industrial facilities.

The high pressure obtained in test no. 9 serves as a reminder that the regular doors of 20-foot ISO containers are not approved explosion venting devices according to EN 14797 (2006). The possibility of generating projectiles during vented deflagrations represents an additional hazard that should be considered in design and risk assessments (Skjold *et al.*, 2017b).

Test no. 14, with venting through the container doors, demonstrates the effect of partly blocking the explosion venting device, and hence reducing the effective vent area (Skjold *et al.*, 2017b).

The dash-dotted blue line in Figure 11 is a linear fit to the experimental results for A_v = 8.0 m^2, with congestion inside the container (pipe rack obstacle in middle position). The fitted curve suggests a significantly steeper increase in pressure, compared to the dotted blue line representing the prediction by the empirical correlations from EN 14994 (2007). Although direct comparison may not be justified, since the experimental results include a wide range of scenarios whereas the standard assumes relatively well defined 'worst-case' conditions, the experimental results indicate a significantly steeper increase in pressure with increasing hydrogen concentration for enclosures with internal congestion, compared to the empirical correlation derived from experiments in empty enclosures.

The results presented here, as well as in related publications (Skjold *et al.*, 2017b; Skjold *et al.,* 2018bcd), should be well suited for model validation (Skjold *et al.*, 2013). However, certain aspects of the experiments should be kept in mind, and ideally accounted for in the analysis:

- From the point of view of vented deflagrations, shipping containers are relatively weak structures, and the typical loading from vented gas explosions with internal congestion can result in complex pressure loads (Baker *et al.*, 1983; Atanga *et al.*, 2018).
- The structural response of the container results in significant variation in the volume of the vented enclosure and may create additional vent areas, e.g. rupture of walls and openings between the steel frame supporting the vent panels and the upper part of the side walls.
- It is not straightforward to measure, nor model, the effect of the structural response, such as oscillating walls and roof, on the rate of combustion inside the enclosure.

In principle it could be possible to support the development of empirical or semi-empirical correlations for vented hydrogen deflagrations with results from CFD simulations. However, results from the blind-prediction benchmark studies organised as part of the HySEA project indicate that the predictive capabilities of the CFD tools, including the users of such tools, need to be significantly improved before this approach can be realised (Skjold *et al.*, 2018cd).

5 Conclusions

This paper presents the results from 66 vented hydrogen deflagration tests in 20-foot ISO containers. The results demonstrate the strong effect internal congestion can have on the maximum reduced explosion pressure in vented deflagrations. Shipping containers are relatively weak structures, and vented explosions with internal congestion result in complex pressure loads. This complicates the analysis and interpretation of the structural response measurements. The overall results should nevertheless be valuable for the development and validation of empirical or semi-empirical correlations suitable for international standards for explosion venting protective systems.

Acknowledgements

The HySEA project receives funding from the Fuel Cells and Hydrogen 2 Joint Undertaking (FCH 2 JU) under grant agreement No 671461. This Joint Undertaking receives support from the European Union's Horizon 2020 research and innovation programme and United Kingdom, Italy, Belgium and Norway. The members of the HySEA consortium gratefully acknowledge the valuable contributions from the members of the HySEA Advisory Board: Simon Jallais and Elena Vyazmina from Air Liquide, Derek Miller from Air Products, Carl Regis Bauwens from FM Global and Y.F. (John) Khalil from United Technologies Research Center (UTRC).

References

Atanga, G., Lakshmipathy, S., Skjold, T., Hisken, H. & Hanssen, A.G. (2018). Structural response for vented hydrogen deflagrations: coupling CFD and FE tools. *International Journal of Hydrogen Energy*, DOI: https://doi.org/10.1016/j.ijhydene.2018.08.085

Baker, W.E., Cox, P.A., Westine, P.S., Kulesz, J.J. & Strehlow, R.A. (1983). *Explosion hazards and evaluation*. Elsevier, Amsterdam.

Carcassi. M., Schiavetti, M. & Pini, T. (2018). Non-homogeneous hydrogen deflagrations in small scale enclosure: Experimental results. *International Journal of Hydrogen Energy*, 43: 19293-19304. DOI: https://doi.org/10.1016/j.ijhydene.2018.08.172

EN 14797 (2006). *Explosion venting devices.* European Committee for Standardization (CEN), Brussels, Belgium: 30 pp.

EN 14994 (2007). *Gas explosion venting protective systems*. European Committee for Standardization (CEN), Brussels, Belgium: 30 pp.

Hisken, H., Atanga, G., Skjold, T., Lakshmipathy, S. & Middha, P. (2016). Validating, documenting and qualifying models used for consequence assessment of hydrogen explosion scenarios. Eleventh International Symposium on Hazards, Prevention and Mitigation of Industrial Explosions (11 ISHPMIE), Dalian, 24-29 July 2016: 1069-1086. ISBN 978-7-89437-165-2. DOI: https://doi.org/10.5281/zenodo.581649

Holtappels, K. (2006). *Report on the experimentally determined explosion limits, explosion pressures and rates of explosion pressure rise, Part 1: methane, hydrogen and propylene.* SAFEKINEX Project Deliverable No. 8, Federal Institute for Materials Research and Testing (BAM), Germany, 149 pp.

Lakshmipathy, S., Skjold, T., Hisken, H. & Atanga, G. (2018). Consequence models for vented hydrogen deflagrations: CFD vs. engineering models. *International Journal of Hydrogen Energy*, DOI: https://doi.org/10.1016/j.ijhydene.2018.08.079

Makarov, D., Hooker, P., Kuznetsov, M. & Molkov, V. (2018). Deflagrations of localised homogeneous and inhomogeneous hydrogen-air mixtures in enclosures. *International Journal of Hydrogen Energy,* 43: 9848-9869.
DOI: https://doi.org/10.1016/j.ijhydene.2018.03.159

NFPA 68 (2018). *Standard on explosion protection by deflagration venting*. National Fire Protection Association (NFPA), Quincy, Massachusetts. ISBN 978-145591896-6.

Pini, T., Grønsund Hanssen, A., Schiavetti, M. & Carcassi, M. (2018). Small scale experiments and FE model validation of structural response during hydrogen vented deflagrations. *International Journal of Hydrogen Energy*,
DOI: https://doi.org/10.1016/j.ijhydene.2018.05.052

Rao, V.C.M. & Wen, J.X. (2018). Numerical modelling of vented lean hydrogen deflagrations in an ISO container. *International Journal of Hydrogen Energy*,
DOI: https://doi.org/10.1016/j.ijhydene.2018.11.093

Savitzky, A. & Golay, J.E. (1964). Smoothing and differentiation of data by simplified least squares. *Analytical Chemistry*, 36: 1627-1639.
DOI: https://doi.org/10.1021/ac60214a047

Schiavetti, M., Pini, T. & Carcassi, M. (2018). The effect of venting process on the progress of a vented deflagration. *International Journal of Hydrogen Energy*,
DOI: https://doi.org/10.1016/j.ijhydene.2018.05.007

Sinha, A., Rao, V.C.M. & Wen, J.X. (2018). Performance evaluation of empirical models for vented lean hydrogen explosions. *International Journal of Hydrogen Energy*, DOI: https://doi.org/10.1016/j.ijhydene.2018.09.101

Skjold, T. (2018). *Experimental investigation of vented hydrogen deflagrations in containers: homogeneous and inhomogeneous mixtures*. Report HySEA-D2-08-2018.

Skjold, T., Hisken, H., Bernard, L., Mauri, L., Atanga, G., Lakshmipathy, S., Pérez, M.L., Carcassi, M., Schiavetti, M., Rao, V.C.M., Sinha, A., Tolias, I.C., Giannissi, S.G., Venetsanos, A.G., Stewart, J.R., Hansen, O.R., Kumar, C., Krumenacker, L., Laviron, F., Jambut, R. & Huser, A. (2018d). Blind-prediction: estimating the consequences of vented hydrogen deflagrations for inhomogeneous mixtures in 20-foot ISO containers. Twelfth International Symposium on Hazards, Prevention and Mitigation of Industrial Explosions (12 ISHPMIE), Kansas City, 12-17 August 2018: 24 pp.

Skjold, T., Hisken, H., Lakshmipathy, S., Atanga, G., Carcassi, M., Schiavetti, M., Stewart, J.R., Newton, A., Hoyes, J.R., Tolias, I.C., Venetsanos, A.G., Hansen, O.R., Geng, J., Huser, A., Helland, S., Jambut, R., Ren, K., Kotchourko, A., Jordan, T., Daubech, J., Lecocq, G., Hanssen, A.G., Kumar, C., Krumenacker, L., Jallais, S., Miller, D. & Bauwens, C.R. (2018c). Blind-prediction: estimating the consequences of vented hydrogen deflagrations for homogeneous mixtures in 20-foot ISO containers. *International Journal of Hydrogen Energy*, DOI: https://doi.org/10.1016/j.ijhydene.2018.06.191

Skjold, T., Hisken, H., Lakshmipathy, S., Atanga, G., van Wingerden, M., Olsen, K.L., Holme, M.N., Turøy, N.M., Mykleby, M & van Wingerden, K. (2017b). Influence of congestion on vented hydrogen deflagrations in 20-foot ISO containers: homogeneous fuel-air mixtures. Twenty-Sixth International Colloquium on the Dynamics of Explosions and Reactive Systems (26 ICDERS), Boston, 30 July – 4 August 2017: 6 pp.

Skjold, T., Hisken, H., Lakshmipathy, S., Atanga, G., van Wingerden, M., Olsen, K.L., Holme, M.N., Turøy, N.M., Mykleby, M. & van Wingerden, K. (2018b). Vented hydrogen deflagrations in containers: effect of congestion for homogeneous and inhomogeneous mixtures. *International Journal of Hydrogen Energy*, DOI: https://doi.org/10.1016/j.ijhydene.2018.10.010

Skjold, T., Pedersen, H.H., Bernard, L., Middha, P., Narasimhamurthy, V.D., Landvik, T., Lea, T & Pesch, L. (2013). A matter of life and death: validating, qualifying and documenting models for simulating flow-related accident scenarios in the process industry. *Chemical Engineering Transactions*, 31: 187-192. DOI: http://dx.doi.org/10.3303/CET1331032

Skjold, T., Siccama, D., Hisken, H., Brambilla, A, Middha, P., Groth, K.M. & LaFleur, A.C. (2017a). 3D risk management for hydrogen installations. *International Journal of Hydrogen Energy*, 42: 7721-7730. DOI: https://doi.org/10.1016/j.ijhydene.2016.07.006

Skjold, T., Souprayen, C. & Dorofeev, S. (2018a). Fires and explosions. *Progress in Energy and Combustion Science*, 64: 2-3. DOI: http://dx.doi.org/10.1016/j.pecs.2017.09.003